Magnetic Arctic Circle in a Square Ice Qubit Lattice

A. D. King,[1] J. Coraux,[2] B. Canals,[2] and N. Rougemaille[2]
[1]D-Wave Systems, Burnaby, British Columbia V5G 4M9, Canada
[2]Université Grenoble Alpes, CNRS, Grenoble INP, Institut Néel, Grenoble 38000, France

(Received 16 March 2023; accepted 15 September 2023; published 16 October 2023)

Under certain boundary conditions, the square ice model exhibits a phase separation in which the core of the system is disordered while its outer region remains ordered. This phenomenon, known as the "arctic circle," has been studied theoretically in combinatorial mathematics and statistical mechanics. Here, we realize the physics of the arctic circle experimentally for the first time, using a programmable lattice of superconducting qubits, and investigate its properties under the prism of a highly frustrated magnet. Our work reveals two unexpected properties. First, the disordered spin manifold confined within the arctic curve is a spin liquid whose average spin texture resembles that of an antivortex, i.e., it is a topologically charged Coulomb phase. Second, monopole quasiparticle excitations, which are totally absent in theoretical works, can be isolated in a phase-separated system. Remarkably, a monopole segregation mechanism is observed, in which the monopoles are sorted according to the magnetic charge and magnetic moment they carry, without the application of an external driving force.

DOI: 10.1103/PhysRevLett.131.166701

Introduction.—The discovery in the 1930s that water ice exhibits a low-temperature residual entropy per molecule [1–4] was a central result in the controversy about the formulation of the third law of thermodynamics [5–8]. This result was also a milestone in statistical mechanics and triggered a wealth of studies on vertex models [9–11]. In that context, one of the most known vertex models is certainly the square ice model. This two-dimensional model does not have any energy scale and is characterized by a zero-point entropy similar to the one of water ice [12]. This model proved to be relevant in highly frustrated magnetism [13–21].

Under certain boundary conditions—the so-called domain wall boundary conditions (DWBCs)—the square ice model has deep roots with problems of combinatorial mathematics, in particular when studying how finite-size square lattices with specific shapes can be tiled with dominos [22]. Because of the extensive degeneracy of its ground state, one might think that boundary conditions have marginal impact on the properties of the square ice model, at least at the thermodynamic limit. They actually have drastic effects. Regardless of the system size, DWBCs induce a phase separation in which the inner region of the system is disordered, whereas the outer region is ordered. Interestingly, the interface separating the two phases has a circular shape, and this exotic behavior has been coined the "arctic circle" phenomenon [23]. After being evidenced in combinatorial mathematics, this phenomenon spread to other disciplines [24–28] and generated intense theoretical works in different fields of physics.

In this Letter, we report the experimental discovery of an arctic circle physics in an artificial frustrated *spin* system consisting of a superconducting flux qubit lattice. Unlike the square ice model or domino tiling problems, a frustrated spin model allows us to introduce an energy scale and hence to excite monopole quasiparticles in a phase-separated system. Our approach leads to the following interesting observations: (i) When brought close to its ground state, our experimental system exhibits a magnetic arctic curve within which the populations of the different vertex types are not uniformly distributed as one would have expected in a conventional spin liquid. (ii) The region within the arctic curve, which is highly disordered and fluctuating, is not the standard Coulomb phase. Instead, it is a Coulomb phase hosting a negative *topological charge*, and its average spin texture resembles the one of an antivortex. (iii) In the low-energy manifold we image, the monopole density does not totally vanish, and a nontrivial monopole segregation occurs, separating them according to their magnetic charge and magnetic moment, without any *applied* external driving force.

Qubit spin ice experiment.—The arctic circle physics is realized experimentally in a $14 \times 14 \times 3$ array of superconducting flux qubits in a quantum annealing processor. Each spin is represented by a ferromagnetically coupled chain of three qubits, which interact via two-body couplers. This general approach has been used to simulate a variety of spin systems [29–32] and was applied to probe an ice physics in the square and kagome geometries with unprecedented capability [33–35]. The particular configuration of three-qubit chains is the direct analog of the kagome embedding used in Ref. [33]. Key for this work, this approach allows control of the boundary conditions using

local fields, which are zero in the interior of the lattice. The qubit lattice emulates the transverse Ising Hamiltonian

$$\mathcal{H} = \mathcal{J}\left(\sum_{\langle ij\rangle} J_{ij}\hat{\sigma}_i^z\hat{\sigma}_j^z + \sum_i h_i\hat{\sigma}_i^z\right) - \Gamma\sum_i \hat{\sigma}_i^x, \qquad (1)$$

where $\hat{\sigma}_i$ are Pauli operators, $\mathcal{J}$ is the magnitude of the classical Ising Hamiltonian, J_{ij} are Ising coupling terms, h_i is a per-qubit longitudinal field, and Γ is a uniform transverse field. Both J_{ij} and h_i can be programmed at will. In contrast to Ref. [34], we use a conventional annealing protocol: at time $t = 0$, $\Gamma \gg \mathcal{J}$. Γ and $\mathcal{J}$ are then respectively reduced and increased as a function of time, until at final time $t_f = 1.024$ ms, $\Gamma \ll \mathcal{J}$, and the system dynamics is frozen. The direction of the Ising spins at the lattice boundaries is set by the local field to induce DWBCs [see the peculiar orientation of the outer black arrows in Fig. 1(a)] and does not fluctuate (large h_i for i at the lattice edges). As our qubit lattice mimics the properties of a spin system, four vertex types, labeled $T_1, \ldots, T_4$, are present [see Fig. 1(b)], in contrast to the square ice model in which only T_1 and T_2 vertices are permitted.

Observation of a magnetic ice curve.—The first key result is the unambiguous experimental observation of an arctic curve in an artificial square ice under DWBCs. To visualize the arctic curve, we collect all measured spin configurations after the annealing protocol and convert them into average vertex maps [see Figs. 1(c) and 1(d)]. Plotting the spatial distribution of T_1 and T_2 vertex densities, a phase separation is evidenced, with a melted core in the inner region of the lattice (made of a highly disordered mixture of T_1 and T_2 vertices), whereas its shell, made of T_2 vertices, has crystallized. What is truly exotic here is that two phases, one ordered (in the shell) and one disordered (in the bulk), *coexist* because of the boundary conditions.

The vertex populations change continuously from the lattice center to the lattice edges. This is quantitatively measured [Figs. 1(e) and 1(f)] by plotting the average vertex density along the lattice diagonal and along the horizontal axis indicated by the two dashed lines in Fig. 1(d). The cuts have bell-shaped profiles for both vertex types, with an extremum at the lattice center matching the expected value in the conventional square ice [dashed lines in Figs. 1(e) and 1(f)]. We note that if the edges crystallize and form ordered patches of type T_2 vertices, each corner of the lattice selects one specific T_2 subtype to comply with the boundary conditions [Figs. 2(a) and 2(b)]. Remarkably, the spatial distribution of the T_2 subtype vertices remains unbalanced even in the interior of the arctic curve [Fig. 2(c)]. This is in sharp contrast with what happens in the conventional square ice spin liquid, in which T_2 subtypes are homogeneously distributed in the lattice [see dashed lines in Figs. 1(e) and 1(f)].

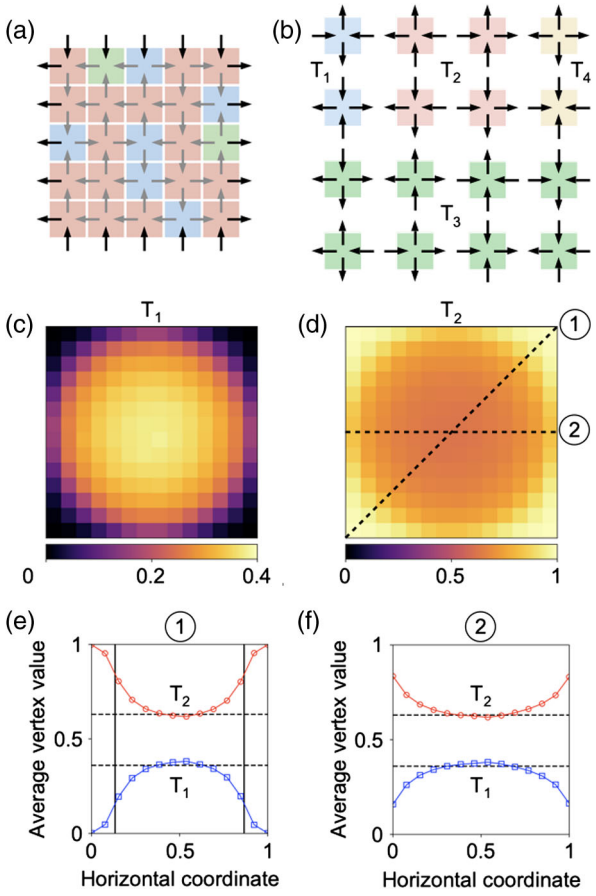

FIG. 1. (a) Schematics of a 5×5 vertex lattice. Spins at the lattice boundaries (in black) are fixed, whereas all other spins (in gray) can fluctuate. (b) The six possible vertex configurations in the square ice ground state manifold are shown in blue (type T_1) and red (type T_2). Single and double monopole excitations (type T_3 and type T_4) appear in green and yellow, respectively. (c), (d) Arctic curve visualized using average vertex maps [type T_1, (c); type T_2, (d)], obtained after the annealing protocol. (e), (f) Vertex populations along the two directions indicated by the dashed lines in (d) for type T_1 (blue curve) and type T_2 (red curve) vertices.

The boundary conditions also forbid the possibility to have the two possible T_1 subtypes in the outer region of the lattice [see Figs. 2(d) and 2(e)]. Counterintuitively, this difference between the T_1 subtypes is not only found in the outer ring of the arctic curve, but extends as well in the interior of the arctic curve [Fig. 2(f)]. There is thus a *systematic* unbalance between the two T_1 subtypes, also in sharp contrast with what is found in the conventional square ice spin liquid [see dashed lines in Figs. 1(e) and 1(f)]. We emphasize that if a vertex unbalance is expected *along* the lattice edges to comply with the boundary conditions, one could have expected the unbalance to be washed out in the interior of the arctic curve, where the phase is extensively degenerate and highly fluctuates. This is not what happens, and the constraints imposed at the lattice edges propagate *throughout* the lattice.

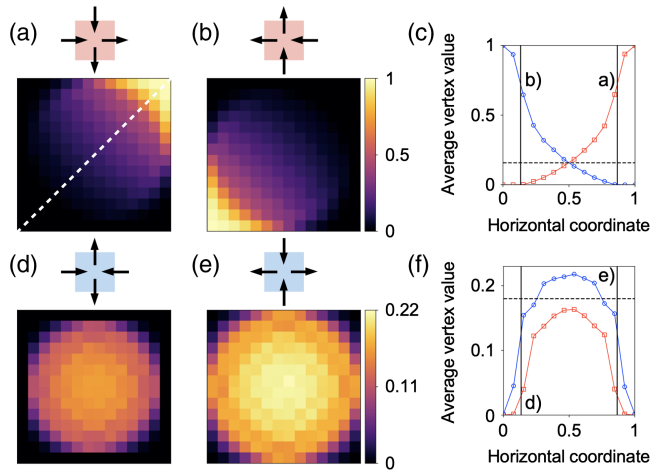

FIG. 2. (a),(b) Average vertex maps for two T_2 subtypes. (c) T_2 subtype populations along the lattice diagonal shown by a white dashed line in (a). (d),(e) Average vertex maps for the two T_1 subtypes. (f) T_1 subtype populations along the lattice diagonal.

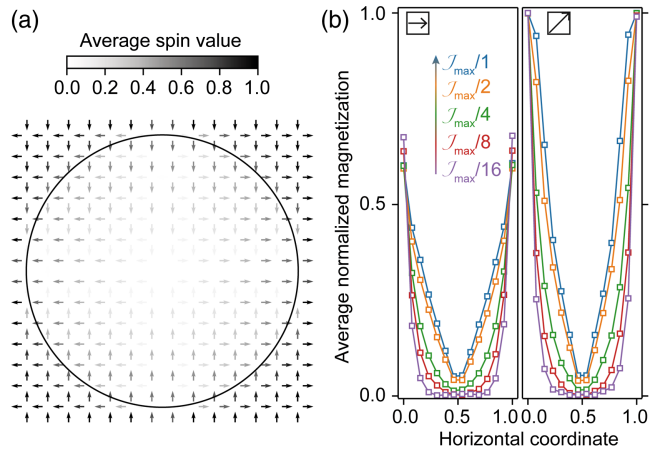

FIG. 3. (a) Spin map obtained when averaging all spin configurations measured after the annealing protocol. The gray scale used for the arrows indicates the average spin value (black for 1, white for 0). This map clearly reveals that the spin value continuously decreases from the edges to the center of the lattice. (b) Average spin value along an horizontal axis going through the lattice center (left panel) and along the lattice diagonal (right panel) for different coupling strengths.

A topologically charged Coulombic spin liquid.—We are then left with this key observation: the domain wall boundary conditions do not solely induce a phase separation, they deeply modify the properties of the Coulomb phase [36] associated with the conventional square ice spin liquid. To characterize the disordered phase we observe, it is instructive to plot the spin texture obtained when averaging all spin configurations measured after the annealing process [see Fig. 3(a)]. In this representation, the gray scale indicates the average spin value. This value is one (black arrow) at the lattice edges due to the DWBCs, whereas it is essentially zero (white arrow) at the lattice center, where the spins fluctuate freely. This representation reveals an interesting property: the average spin value continuously increases from the lattice center to the edges, and does not vary abruptly from 0 to 1 when crossing the arctic curve. Here as well, the DWBCs impose a constraint that propagates throughout the entire lattice. The average spin texture then resembles the field distribution of an antivortex, and the DWBCs confer a (negative) topological charge to the Coulombic spin liquid.

The (theoretical) functional form of the spatial dependence of this average spin texture is unknown. With our experimental approach, however, we can measure this spatial dependence for different coupling strengths $\mathcal{J}$ to visualize the impact of thermal fluctuations [see Fig. 3(b)]. As $\mathcal{J}$ is reduced, the average spin texture fluctuates more and ultimately vanishes for low $\mathcal{J}$ values. This is clearly visible for the lowest $\mathcal{J}$: the average spin values are essentially zero, except very close to the lattice edges, demonstrating that the arctic curve phenomenon disappears when thermal fluctuations dominate [see the purple points in Fig. 3(b) and Sec. I of the Supplemental Material [37]]. We also emphasize that the arctic curve phenomenon is essentially size independent and similar results are expected even for smaller lattice sizes (see Sec. II of the Supplemental Material [37]).

Monopole segregation.—These observations raise another question. The magnetic excitations living on the square ice spin liquid are known to behave as classical analogs of magnetic monopoles, i.e., magnetically charged deconfined quasiparticles [43,44], interacting via a Coulomb potential at long distances. We might then wonder whether monopoles are uniformly distributed in the lattice, like in the conventional square ice spin liquid, or if they are inhomogeneously distributed like the T_1 and T_2 vertices. To answer this question, a density map of type T_3 vertices has been generated from our measurements [Fig. 4(a)].

First of all, we stress that the fraction of T_3 vertices is only 0.0057. This means that around 50% of the probed spin configurations are *truly* in the ground state, while the remaining configurations contain typically *one* excitation (i.e., a single monopole pair). The effective temperature is thus finite but extremely low, and the properties of the system are those of the ground state with very rare monopole excitations.

Unexpectedly, the map reported in Fig. 4(a) reveals that the magnetic monopoles remaining trapped in the lattice are localized in very specific regions, along the arctic curve, in the vicinity of the lattice edges. The density maps for the eight monopole subtypes [Fig. 4(b)] show another puzzling result: the monopoles are sorted according to the *magnetic charge* they carry [the upper and lower rows in Fig. 4(b) correspond to positive and negative magnetic charges, respectively]. Positive magnetic charges accumulate on the top and bottom edges of the lattice, whereas negative magnetic charges accumulate along the right and left sides.

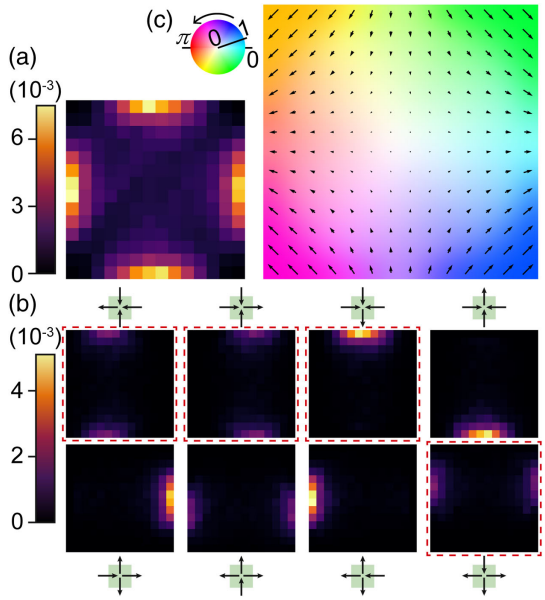

FIG. 4. (a) Experimental average vertex map for all eight T_3 vertices. (b) Average vertex maps for all individual T_3 vertices, showing that each vertex has a specific spatial distribution. Red dashed frame indicates the four monopoles having their upper spin aligned with the one of the upper lattice edge. (c) Colored map showing the average value and average direction of the magnetic moment carried by the vertices. The map demonstrates that the topological charge induced by the DWBCs propagates in the interior of the arctic curve.

What is remarkable here is that monopoles carrying the *same* magnetic charge move in opposite directions! This is in sharp contrast with what can be done with an applied external magnetic field [45–50].

Besides the magnetic charge, the monopoles are sorted as well according to the *magnetic moment* they carry. For example, considering only the four positively charged monopoles [upper row in Fig. 4(b)], a moment selection is clearly evidenced, and each of the four vertex maps differs from the others. The arctic circle in our ice magnet also acts as a monopole moment selector. We emphasize that these two selection mechanisms occur without the application of an external driving force.

The physical origin of the charge and moment selection is linked to the constraint imposed by the domain wall boundary conditions. Considering the top vertex row in Fig. 1(a), the upper spins are fixed and point downward. Thus, only four of the eight possible monopoles can exist along this vertex row. Among these four monopoles, three are positively charged and one is negatively charged [see maps in Fig. 4(b)]. From that perspective alone, we expect the upper part of the lattice to be positively charged on average (as observed experimentally). In addition, one should keep in mind that thermally generated monopoles cannot escape the lattice from the edges, and monopoles can only annihilate with oppositely charged ones. Because of the imbalance between the two monopole charges at the lattice edges, we then also expect the minority charge (negative in the upper part of the lattice) to ultimately disappear at low temperature after recombination with the majority charges. Positive magnetic charges thus accumulate on the upper and lower lattice edges, whereas negative charges accumulate on the right and left sides.

One might argue that the above explanation is only valid *at* the lattice edges. However, as discussed above, the topological charge imposed by the DWBCs propagates in the interior of the arctic curve. As a consequence, charge selection also occurs there, although the mechanism becomes less and less efficient as the distance from the edges increases and the system fluctuates more. This is in fact visible in the vertex map shown in Fig. 4(a), in which a nonzero monopole density is observed away from the lattice edges for all T_3 subtypes. This effect is even better visualized when plotting the T_3 density maps for different coupling strengths. If the monopole density is rather homogeneously distributed when thermal fluctuations are large, the rare monopoles that are trapped remain at (or very close to) the lattice edges where they cannot annihilate anymore with their antimonopole (see Sec. III of the Supplemental Material [37]).

The presence of a topologically charged spin texture explains as well why the monopoles are sorted according to their magnetic moment. This is again directly visible in the vertex maps reported in Fig. 4(b). For example, the three positively charged monopoles in red-framed maps have a magnetic moment pointing along the [-10], [10], and [0-1] directions, and are positioned in regions where the underlying spin texture carries a substantial magnetic moment along these directions [see Fig. 4(c)]. In that sense, the monopole moments interact with the spin texture on top of which they live. The spatial distribution of the T_3 densities reflects the topological nature of the Coulombic spin liquid, conferring specific properties to the monopoles that are not found in other systems (see Sec. III of the Supplemental Material [37]).

Prospects.—A question that naturally comes to mind is whether the arctic curve phenomenon holds for boundary conditions other than the T_1-like DWBCs. We hence implemented T_2-, T_3-, and T_4-like boundary constraints in our superconducting qubit lattice, and observed different interfaces between the (sometimes partially) melted core and the ordered shell (see Sec. IV of the Supplemental Material [37]). Noteworthy, under T_4 boundary conditions, the average spin texture resembles the one of a two-dimensional Néel-like magnetic skyrmion, thus carrying a positive topological charge. Potentially new physics might be at play under such conditions, calling for further investigations.

We might also wonder to what extent an external applied magnetic field would affect the charge and moment distributions of the monopoles within the topologically charged Coulombic spin liquid. Understanding whether an

applied field could counterbalance the monopole selection mechanism or facilitate monopole recombination processes would definitively be an interesting route to pursue in future works. By tracking the monopole motion in time, such experiments might in particular be useful to identify potential nonequilibrium phenomena in the selection mechanism we observed.

Finally, the arctic curve phenomenon might be explored in artificial spin ice systems [18], provided that the spin states at the lattice boundaries can be set and fixed independently of all the other spins. If this is achieved, investigating what happens in other geometries (kagome, pinwheel, or Shakti to name only a few [51]) could open the door to a panoply of new effects.

This work was supported by the Agence Nationale de la Recherche through Projects No. ANR-17-CE24-0007-03 "Bio-Ice" and ANR-22-CE30-0041-01 "ArtMat." N. R. and B. C. thank Lucas Reneuve for fruitful discussions.

[1] W. F. Giauque and M. F. Ashley, Phys. Rev. **43**, 81 (1933).
[2] W. F. Giauque and J. W. Stout, J. Am. Chem. Soc. **58**, 1144 (1936).
[3] J. D. Bernal and R. H. Fowler, J. Chem. Phys. **1**, 515 (1933).
[4] L. Pauling, J. Am. Chem. Soc. **57**, 2680 (1935).
[5] F. E. Simon, Z. Naturforsch. A **6**, 397 (1951).
[6] A. J. Kox, Stud. Hist. Phil. Mod. Phys. **37**, 101 (2006).
[7] A. Y. Klimenko, Open Thermodyn. J. **6**, 1 (2012).
[8] M. Aizenman and E. H. Lieb, J. Stat. Phys. **24**, 279 (1981).
[9] R. J. Baxter, *Exactly Solved Models in Statistical Mechanics* (Academic Press Limited, London, 1982).
[10] E. H. Lieb, *Statistical Mechanics* (Springer-Verlag, Berlin, 2004).
[11] P. Zinn-Justin, arXiv:0901.0665.
[12] E. Lieb, Phys. Rev. **162**, 162 (1967).
[13] S. T. Bramwell, M. J. P. Gingras, and P. C. W. Holdsworth, in *Frustrated Spin Systems*, edited by H. T. Diep (World Scientific Book, Singapore, 2013).
[14] S. T. Bramwell and M. J. Harris, J. Phys. Condens. Matter **32**, 374010 (2020).
[15] Y. Perrin, B. Canals, and N. Rougemaille, Nature (London) **540**, 410 (2016).
[16] E. Östman, H. Stopfel, I.-A. Chioar, U. B. Arnalds, A. Stein, V. Kapaklis, and B. Hjörvarsson, Nat. Phys. **14**, 375 (2018).
[17] A. Farhan, M. Saccone, C. F. Petersen, S. Dhuey, R. V. Chopdekar, Y.-L. Huang, N. Kent, Z. Chen, M. J. Alava, T. Lippert, A. Scholl, and S. van Dijken, Sci. Adv. **5**, eaav6380 (2019).
[18] N. Rougemaille and B. Canals, Eur. Phys. J. B **92**, 62 (2019).
[19] O. Brunn, Y. Perrin, B. Canals, and N. Rougemaille, Phys. Rev. B **103**, 094405 (2021).
[20] M. Goryca, X. Zhang, J. Li, A. L. Balk, J. D. Watts, C. Leighton, C. Nisoli, P. Schiffer, and S. A. Crooker, Phys. Rev. X **11**, 011042 (2021).
[21] V. Schánilec, O. Brunn, M. Horáček, S. Krátký, P. Meluzín, T. Šikola, B. Canals, and N. Rougemaille, Phys. Rev. Lett. **129**, 027202 (2022).
[22] I. N. Elkies, G. Kuperberg, M. Larsen, and J. Propp, J. Algebraic Combin. **1**, 111 (1992).
[23] W. Jockush, J. Propp, and P. Shor, arXiv:math/9801068.
[24] K. Johansson, Probab. Theory Relat. Fields **123**, 225 (2002).
[25] V. Korepin and P. Zinn-Justin, J. Phys. A **33**, 7053 (2000).
[26] R. Kenyon, A. Okounkov, and S. Sheffield, Ann. Math. **163**, 1019 (2006).
[27] L. F. Cugliandolo, G. Gonnella, and A. Pelizzola, J. Stat. Mech. (2015) P06008.
[28] L. F. Cugliandolo, J. Stat. Phys. **167**, 499 (2017).
[29] R. Harris, Y. Sato, A. J. Berkley, M. Reis, F. Altomare, M. H. Amin, K. Boothby, P. I. Bunyk, C. Deng, C. Enderud *et al.*, Science **361**, 162 (2018).
[30] A. D. King, J. Carrasquilla, J. Raymond, I. Ozfidan, E. Andriyash, A. J. Berkley, M. Reis, T. Lanting, R. Harris, F. Altomare *et al.*, Nature (London) **560**, 456 (2018).
[31] P. Weinberg, M. Tylutki, J. M. Rönkkö, J. Westerholm, J. A. Åström, P. Manninen, P. Törmä, and A. W. Sandvik, Phys. Rev. Lett. **124**, 090502 (2020).
[32] A. D. King, J. Raymond, T. Lanting, S. V. Isakov, M. Mohseni, G. Poulin-Lamarre, S. Ejtemaee, W. Bernoudy, I. Ozfidan, A. Y. Smirnov *et al.*, Nat. Commun. **12**, 1113 (2021).
[33] A. Lopez-Bezanilla, J. Raymond, K. Boothby, J. Carrasquilla, C. Nisoli, and A. D. King, Nat. Commun. **14**, 1105 (2023).
[34] A. D. King, C. Nisoli, E. D. Dahl, G. Poulin-Lamarre, and A. Lopez-Bezanilla, Science **373**, 576 (2021).
[35] S. Zhou, D. Green, E. D. Dahl, and C. Chamon, Phys. Rev. B **104**, L081107 (2021).
[36] C. L. Henley, Annu. Rev. Condens. Matter Phys. **1**, 179–210 (2010).
[37] See Supplemental Material at http://link.aps.org/supplemental/10.1103/PhysRevLett.131.166701 for details on the impact of the coupling strength, on the lattice size, on the monopole segregation mechanism, and on the influence of the boundary conditions, which includes Refs. [38–42].
[38] R. F. Wang, C. Nisoli, R. S. Freitas, J. Li, W. McConville, B. J. Cooley, M. S. Lund, N. Samarth, C. Leighton, V. H. Crespi, and P. Schiffer, Nature (London) **439**, 303 (2006).
[39] J. P. Morgan, A. Stein, S. Langridge, and C. H. Marrows, Nat. Phys. **7**, 75 (2011).
[40] Z. Budrikis, J. P. Morgan, J. Akerman, A. Stein, Paolo Politi, S. Langridge, C. H. Marrows, and R. L. Stamps, Phys. Rev. Lett. **109**, 037203 (2012).
[41] A. Farhan, P. M. Derlet, A. Kleibert, A. Balan, R. V. Chopdekar, M. Wyss, J. Perron, A. Scholl, F. Nolting, and L. J. Heyderman, Phys. Rev. Lett. **111**, 057204 (2013).
[42] J. M. Porro, A. Bedoya-Pinto, A. Berger, and P. Vavassori, New J. Phys. **15**, 055012 (2013).
[43] I. A. Ryzhkin, J. Exp. Theor. Phys. **101**, 481 (2005).
[44] C. Castelnovo, R. Moessner, and S. L. Sondhi, Nature (London) **451**, 42 (2008).
[45] S. Ladak, D. E. Read, G. K. Perkins, L. F. Cohen, and W. R. Branford, Nat. Phys. **6**, 359 (2010).
[46] E. Mengotti, L. J. Heyderman, A. Fraile Rodríguez, F. Nolting, R. V. Hügli, and H.-B. Braun, Nat. Phys. **7**, 68 (2011).

[47] J. P. Morgan, A Stein, S Langridge, and C H Marrows, New J. Phys. **13**, 105002 (2011).
[48] C. Phatak, A. K. Petford-Long, O. Heinonen, M. Tanase, and M. De Graef, Phys. Rev. B **83**, 174431 (2011).
[49] S. D. Pollard, V. Volkov, and Y. Zhu, Phys. Rev. B **85**, 180402(R) (2012).
[50] S. A. Morley, J. M. Porro, A. Hrabec, M. C. Rosamond, D. A. Venero, E. H. Linfield, G. Burnell, M.-Y. Im, P. Fischer, S. Langridge, and C. H. Marrows, Sci. Rep. **9**, 15989 (2019).
[51] S. H. Skjærvø, C. H. Marrows, R. L. Stamps, and L. J. Heyderman, Nat. Rev. Phys. **2**, 13 (2020).